SCIENTIFIC REPORTS

OPEN

SUBJECT AREAS:
METALS AND ALLOYS
MECHANICAL PROPERTIES
CONDENSED-MATTER PHYSICS
NANOSCALE MATERIALS

Received
19 September 2012

Accepted
1 February 2013

Published
22 February 2013

Correspondence and requests for materials should be addressed to C.T.L. (chainliu@cityu.edu.hk)

# A nanoscale co-precipitation approach for property enhancement of Fe-base alloys

Zhongwu Zhang[1,2,3], Chain Tsuan Liu[4], Michael K. Miller[2], Xun-Li Wang[5], Yuren Wen[6], Takeshi Fujita[6], Akihiko Hirata[6], Mingwei Chen[6], Guang Chen[7] & Bryan A. Chin[1]

[1]Materials Research & Education Center, Auburn University, 275 Wilmore Labs, Auburn, AL 36849, USA, [2]Oak Ridge National Laboratory, Oak Ridge, TN 37831, USA, [3]Kay Laboratory of Superlight Materials and Surface Technology, Ministry of Education, Harbin Engineering University, Harbin 150001, P.R. China, [4]Center for Advanced Structural Materials, College of Science and Engineering, City University of Hong Kong, Kowloon, Hong Kong, [5]Department of Physics and Materials Science, City University of Hong Kong, Kowloon, Hong Kong, [6]WPI Advanced Institute for Materials Research, Tohoku University, Sendai 980-8577, Japan, [7]EMBD, Ministry of Education, Nanjing University of Science and Technology, Nanjing 210094, P. R. China.

**Precipitate size and number density are two key factors for tailoring the mechanical behavior of nanoscale precipitate-hardened alloys. However, during thermal aging, the precipitate size and number density change, leading to either poor strength or high strength but significantly reduced ductility. Here we demonstrate, by producing nanoscale co-precipitates in composition-optimized multicomponent precipitation-hardened alloys, a unique approach to improve the stability of the alloy against thermal aging and hence the mechanical properties. Our study provides compelling experimental evidence that these nanoscale co-precipitates consist of a Cu-enriched bcc core partially encased by a B2-ordered Ni(Mn, Al) phase. This co-precipitate provides a more complex obstacle for dislocation movement due to atomic ordering together with interphases, resulting in a high yield strength alloy without sacrificing alloy ductility.**

Precipitate-hardening (PH) is one of the most effective strengthening methods used in modern aerospace, automotive and construction materials[1–5]. It is well known that conventional PH requires an optimized combination of precipitate size and number density to yield the maximum combination of properties, such as yield strength, hardness, and ductility[6]. However due to the limited supply of solutes, the precipitate size and number density are controlled by the solubility limits and heat treatment. During conventional aging or service conditions, structural evolution is dictated by the nucleation of a high number density of small precipitates, or a lower number density of larger precipitates by an Oswald ripening mechanism[6]. This aging response results in either high strength, but generally with a significant reduction in ductility or poor strength with a slight increase in ductility after overaging[7–10].

This study offers a fundamentally new strategy to alloy strengthening, in which a small change in alloy composition can lead to a substantial improvement in the strength without sacrificing the ductility, through the formation of nanoscale co-precipitates with a Cu-enriched bcc core partially encased by a B2-ordered Ni(Mn, Al) phase. This proof-of-concept study is based on a new class of high-strength Fe-based PH alloys[10–13] with a base composition of Fe-2.5Cu-2.1Al-1.5Mn (at.%). Two different Ni additions were used, 2.5% Ni (hereafter designated as the low nickel alloy) and 4% Ni (designated as the high nickel alloy) to demonstrate the effect. The Cu-enriched/ordered B2-Ni(Mn, Al) co-precipitates were produced in this alloy by a combination of controlled nucleation of precipitates and subsequent solute separation. The nucleation of precipitates is mainly controlled by the Cu content whereas suitable Ni content and aging scheme induce a separation of a Cu-enriched core and ordered B2-Ni(Mn, Al) phase, leading to the formation of co-precipitates.

The formation of these ~4-nm co-precipitates was revealed by a combination of advanced electron microscopy for structural analyses and by atom probe tomography (APT) for visualizing the solute distribution with both atomic resolution and elemental sensitivity. The nature and crystallographic structure of the Cu-rich nanoprecipitates with diameters less than 4 nm has been a subject of debate for many years[6,14–23]. A commonly-accepted view is that the supersaturated copper atoms initially precipitate out as a metastable body-centered-cubic (bcc) phase which is coherent with the α–Fe matrix[15]. Plane matching experiments in atom probe field ion microscopy also support a bcc structure[24]. During subsequent growth, the precipitates transition through faulted structures of

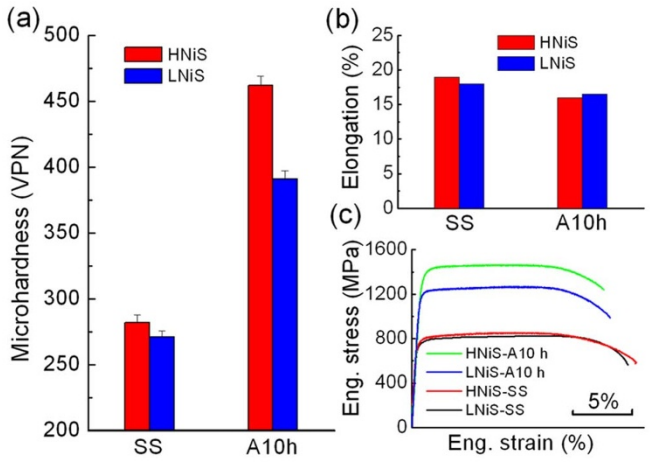


**Figure 1 | Microhardness, ductility to failure, and stress-strain curves for the low and high nickel steels (LNiS and HNiS) for both the solid solution (SS) and after aging for 10 h at 500°C in vacuum (A10h).**

hexagonally-ordered phases (9R and 3R), and finally become the equilibrium face-centered-cubic (fcc) structure of ε-copper[19]. For multicomponent Fe-based alloys, solutes Ni, Al and Mn may be used in combination to refine the grain size and strengthen the grain boundaries and matrix[6,11,13]. During aging, these alloying additions may produce additional phases, such as B2-ordered FeAl or NiAl, and these solute elements can be rejected from the Cu-enriched nucleus and then accumulate at the particle/matrix interfaces[14,25]. X-ray synchrotron diffraction has been used to examine the formation of an ordered B2 Ni (AlMn) phase after long aging times[17] . However, these analyses were performed only for relatively large nanoscale precipitates with sizes significantly >5 nm. Moreover, synchrotron diffraction can only give the average phase information but not nanoscale chemical distribution of the B2-ordered structure.

The ability to resolve spatially the atomic–scale structure and solute distributions at the nanoscale would greatly advance our understanding of the correlation between the microstructures and the resulting properties in materials. This information is particularly important to nanoscale precipitates with a complicated structure, as dislocation movement will be profoundly affected by such precipitate morphology. In addition, the coarsening of the complicated precipitates could be impeded. In this study, the atomic structure and chemistry of the nanoprecipitates in these alloys were characterized by complementary atom probe tomography (APT) together with the state-of-the-art Cs-corrected transmission electron microscopy (TEM), scanning TEM (STEM) with ultra-high spatial resolutions of ~1Å.

## Results

The microhardness, ductility, and typical stress-strain curves are shown in Fig. 1 for both alloys in the solid solution state and the precipitation state produced by aging for 10 h at 500°C in vacuum. The values are shown in Table 1. In the solid solution state, in which there are no nanoprecipitates, the yield strengths of both low nickel and high nickel alloys are comparable at ~735 MPa, regardless of the Ni contents. Upon aging, the yield strengths increased dramatically to ~1168 and 1363 MPa for the low and high nickel alloys, respectively. Therefore, the addition of an extra 1.5% Ni induces a 45% increase in yield strength upon aging while maintaining a ductility of ~16%. This improvement in mechanical properties demonstrates the significant effect of Ni on the mechanical properties.

Neutron powder diffraction spectra from both the low and high nickel alloy specimens show a typical single phase bcc structure of ferrite to within ~1% experimental precision. Optical microscopy revealed that both alloys have a similar microstructure, with an average grain size of ~10 μm, and there is no appreciable change after aging. This indicates that both alloys were fully recrystallized during solid solution treating at 900°C. To explore the underlying mechanism of the significant difference in yield strength induced by the addition of extra Ni, the fine scale microstructure was analyzed by APT. As shown in Fig. 2, a large amount of precipitates are embedded in the ferrite matrix. These precipitates mainly consist of solutes Cu, Ni, Al and Mn. Although Cu-enriched precipitates have been reported previously[10,11], the precipitates in these alloys exhibited a characteristic co-precipitation structure in the high nickel alloy, as shown in Fig. 3. One-dimensional concentration profiles of the constituent elements through the center of these co-precipitates, together with 11 at.% Cu and 9 at.% Ni isoconcentration surfaces, are shown in Fig. 3. The threshold values of Cu (11 at.%) and Ni (9 at.%) isosurfaces were selected to make sure some parts of Cu and Ni isosurfaces in the largest precipitates can be coincident (left hand-side precipitates in Fig. 3b). In both of the low and high nickel alloys, Fe is depleted in the precipitates. In the low nickel alloy (Fig. 3a), Ni, together with Al and Mn, mainly segregated in the precipitate core and there is a more pronounced difference in the Ni distribution in the high nickel alloy, as shown in Fig. 3b. The statistical fluctuations of the precipitate size and solutes segregation induce different precipitate structures. In some smaller precipitates, the Ni and Al are quite uniformly distributed inside, and around the Cu-enriched core, the Ni(Al)-enriched shell is gradually formed (e.g., the particle at right-hand side in Fig. 3b). At larger sizes, the distributions of Cu, Ni and Al change. The Cu-enriched core becomes more enriched in copper and the Ni and Al are further rejected from the core and become enriched along some preferred directions, as shown in Fig. 3b (e.g., the particle at left-hand side), forming co-precipitates. This co-precipitation is different from the case in which the Cu dissolved in the NiAl phase, as demonstrated in a Cu-containing maraging stainless steel, where the Ni concentration is as high as 10% weight percent[26]. The one-dimensional concentration profile clearly shows a Ni and Al peaks adjacent to a Cu peak, as indicated by the arrows in the top right-hand side of Fig. 3b, demonstrating the formation of a co-precipitates. This case was not observed in the low nickel alloy. The difference of nano-scale phase separation between the low and high nickel alloys also clearly demonstrated in Fig. 3 in the isoconcentration surfaces. In low nickel alloy, the 9 at.% Ni isoconcentration surface is located inside or is coincident with the

Table 1 | Mechanical properties and precipitate parameters for the low and high nickel alloys (LNiS and HNiS) for both the solid solution (SS) and after aging for 10 h at 500°C in vacuum (A10 h). A 2000 h denotes a high nickel alloy after aging for 2000 h at 500°C

| | Aging condition | Hardness (VPN) | Elongation to failure% | YS MPa | UTS MPa | Radius Cu nm | Radius Ni nm | Number density $10^{24}$ $m^{-3}$ |
|---|---|---|---|---|---|---|---|---|
| HNiS (4 wt.% Ni) | SS | 282 ± 6 | 19 | 741 | 849 | N/A | N/A | N/A |
| | A10 h | 462 ± 7 | 16 | 1363 | 1457 | 1.3 ± 0.18 | 1.6 ± 0.34 | 3.6 |
| | A2000 h | N/A | N/A | N/A | N/A | 2.5 ± 1 | 5 ± 3 | 0.1 |
| LNiS (2.5 wt.% Ni) | SS | 271 ± 5 | 18 | 734 | 829 | N/A | N/A | N/A |
| | A10 h | 391 ± 6 | 16.5 | 1168 | 1266 | 1.3 ± 0.25 | 1.3 ± 0.32 | 3.6 |

11 at.% Cu isoconcentation surface. In contrast, in the high nickel alloy, the extent of the 9 at.% Ni isoconcentration surface is larger than that of the 11 at.% Cu isoconcentation surface. Non-uniform distributions of Ni and Al around the Cu-enriched core are also clearly demonstrated in the isoconcentration surface in Fig 3b.

APT results in Table 1 show that the Cu-enriched cores in both alloys have a similar average radius of ~1.3 nm and number density $3.6 \times 10^{24}$ $m^{-3}$. However, the co-precipitates in the high nickel alloy are far more extended spatially, with an average radius reaching ~1.6 nm due to the formation of the Ni- and Al-enriched shell. These results confirm that the increases in yield strength in both low and high nickel alloys are mainly due to the formation of nano-scale co-precipitates. To learn the evolution of the co-precipitation structure with aging time, high nickel alloys were aged at 500°C for 2000 h. Elemental mapping of a typical precipitate, together with one-dimensional concentration profiles of the constituent elements through the center of this precipitate are shown in Fig. 4. After long time aging, the precipitate grew but the co-precipitation structure is still remained. The Cu-rich core grew to an average of ~2.5 nm in radius, which is reasonably larger than ~1.3 nm in the alloy aged for 10 h (Table 1), and the NiAl(Mn)-enriched phase is more evident. In addition, the number density of precipitates decreases to $\sim 0.1 \times 10^{24}$ $m^{-3}$, one order of magnitude lower than that in the alloy aged for 10 h (Table 1). It should be noted that the number density in a similar alloy with 2.0 wt.% Cu and lower Ni (2.8 wt.%) was determined to be only $7.5 \times 10^{22}$ $m^{-3}$ after aging for 1024 h[6]. This indicates that the existence of the NiAl(Mn) phase around the Cu-enriched core can effectively retard the growth and coarsening of the precipitates. The development of the chemical composition of the Cu-enriched core indicates that the concentration of Cu in the Cu-enriched core increases significantly to ~90% Cu at the core center and the atom ratio of Ni and Al in NiAl(Mn)-enriched shell approaches to 1 : 1 (Fig. 4b) after aging for 2000 h.

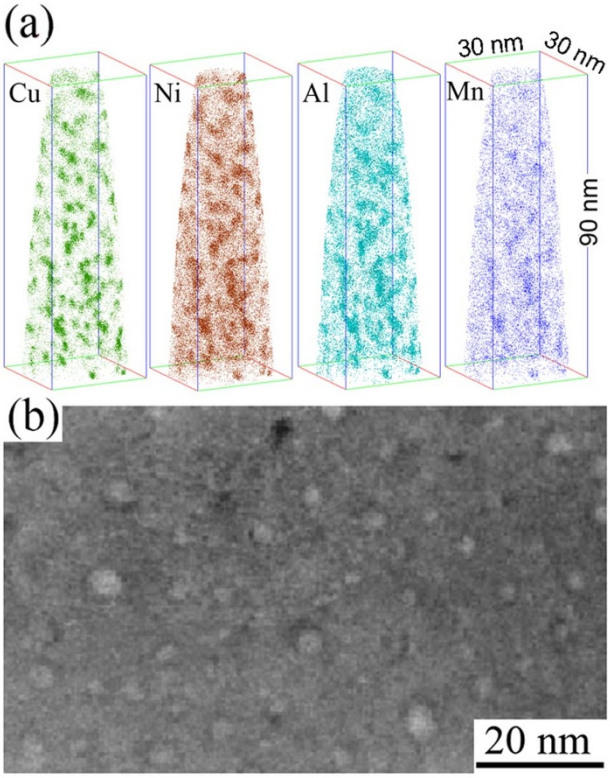


**Figure 2** | (a) Typical APT reconstruction of the high nickel alloy after aging at 500°C for 10 h in vacuum. The atom maps indicate that well-defined spheroidal precipitates are enriched with solute Cu, Ni, Al and Mn. (b) HAADF image of the precipitate distribution in the high nickel alloy after aging at 500°C for 10 h in vacuum.

To further characterize the nanoscale precipitate structure, a systematic microscopy study was conducted with an aberration-corrected scanning transmission electron microscope (STEM). A typical HAADF-STEM image of a duplex precipitate in the high nickel alloy after aging at 500 C for 10 h, is shown in Fig. 5a. HAADF-STEM image mainly shows the mass contrast, where the regions with lower-density and/or lighter elements exhibit darker contrast and vice versa[3]. The brighter 3-5-nm-diameter central region corresponds to a Cu-enriched core and the dark periphery indicates the formation of a second phase. All of these agree with the APT measurements (Fig. 3b). The detailed solute distribution in the co-precipitates was investigated by electron-energy-loss spectroscopy (EELS) in the STEM mode, as shown in Figs. 5b–d. A Cu-enriched (marked by dash line in Fig. 5c) and Fe-depleted region (Fig. 4b) partially surrounded by a Ni-enriched region (marked by dash line in Fig. 5d), is clearly seen. This observation is consistent with the APT data.

A typical low-pass filtered high resolution HAADF image of a co-precipitate taken with the electron beam parallel to the $[001]_{\alpha\text{-Fe}}$ direction from the high nickel alloy is shown in Fig. 4e. Even though there is only a weak contrast variation, the precipitate exhibited slightly brighter contrast. The radius of the precipitate was ~2 nm and was comparable to the size estimated by APT. A well-developed co-precipitation structure of the precipitate can be identified from the contrast difference between the brighter Cu-enriched core region and the darker peripheral region. This is consistent again with APT results (Fig. 3b). To understand the crystalline structure of the nano-precipitates, fast Fourer transform (FFT) analysis was conducted from the selected area as marked in the atomic-resolution STEM image in Fig. 5e. Based on the FFT analysis (Fig. 5f), the crystal structure of the Cu-rich core was found to have a distorted bcc structure, which is also confirmed by the periodicity of the atom columns in the STEM image. An ordered $(010)_{B2}$ reflection can be clearly seen in FFT pattern in the peripheral region, indicating unambiguously that this phase has an ordered B2 (CsCl) structure.

## Discussion

The aging response is different for the low and high nickel alloys due to the different Ni contents, resulting in quite different mechanical properties. APT results show that for both low and high nickel alloys, a similar number density and Cu-enriched core size were obtained after aging for 10 h (Table 1). This indicates that the nucleation of the precipitates is controlled mainly by Cu content since both low and high nickel alloys have the same Cu content. The difference in Ni contents, however, leads to a different precipitate structure which contributes to the mechanical properties difference. Ni is mainly dissolved in the Cu-enriched core with low Ni additions whereas high Ni additions results in the separation of Ni from Cu-enriched core, forming co-precipitates with Cu-enriched core encased by Ni-enriched phase. Based on the APT and TEM results, it can be concluded that this Ni-enriched phase around the Cu-enriched core is enriched with Ni, Al and Mn, forming an ordered B2 phase. This Ni-Al-enriched ordered B2 phase corresponds to a nonstoichiometric intermetallic compound with a very broad compositional range from Al-45 at.% Ni to Al-58 at.%Ni in the equilibrium Ni-Al phase diagram. Thus, this B2 structure exhibits chemical flexibility with multiple constituent elements, specifically, Mn substituting at Al sublattice sites as demonstrated by first-principles calculations[17], forming the B2-Ni(Mn,Al) phase. ALCHEMI and APT studies have also indicated that the NiAl ordered B2 phase can accommodate other solutes, such as Fe[27]. With aging, the Fe, Ni and Al are rejected further from the Cu-enriched core leading to a significant increase in the Cu concentration while the B2-NiAl phase changes towards the stoichiometric composition.

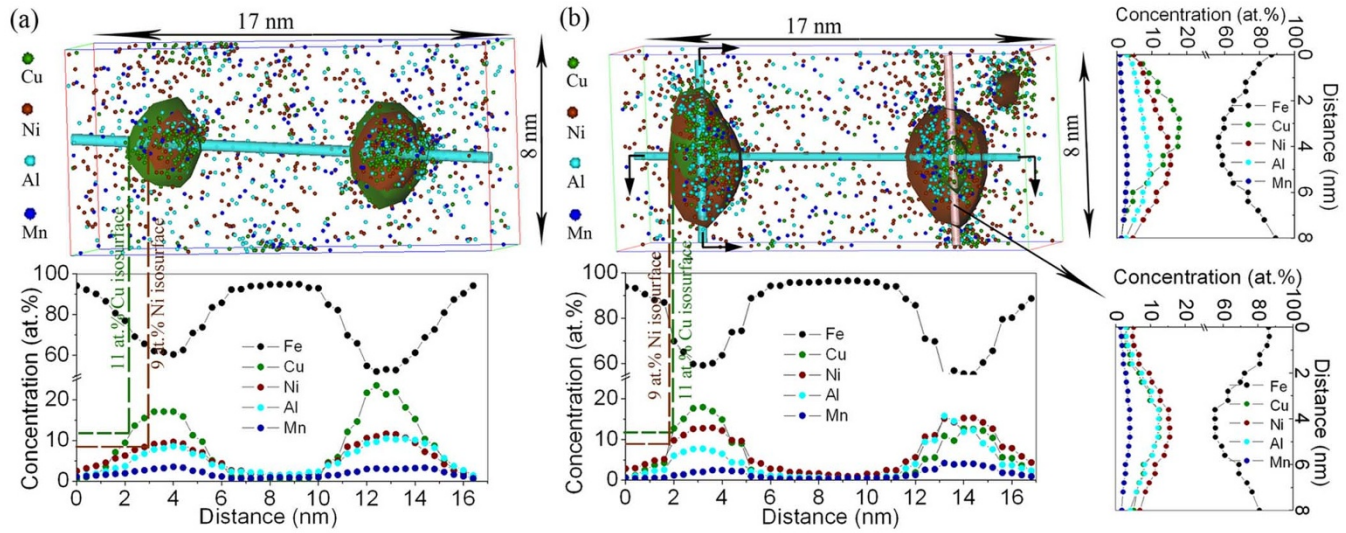


**Figure 3 | Concentration distributions and atoms maps with 11 at.% Cu and 9 at.% Ni isoconcentration surfaces of 2 precipitates reconstructed from the APT data showing the profiles of elements distribution for (a) low nickel alloy and (b) high nickel alloy after aging at 500°C for 10 h in vacuum.** Atom maps show that Ni mainly segregates into the precipitate core in the low nickel alloy, whereas, Ni distributes uniformly around the small Cu-enriched cores and non-uniformly for larger cores in the high nickel alloy.

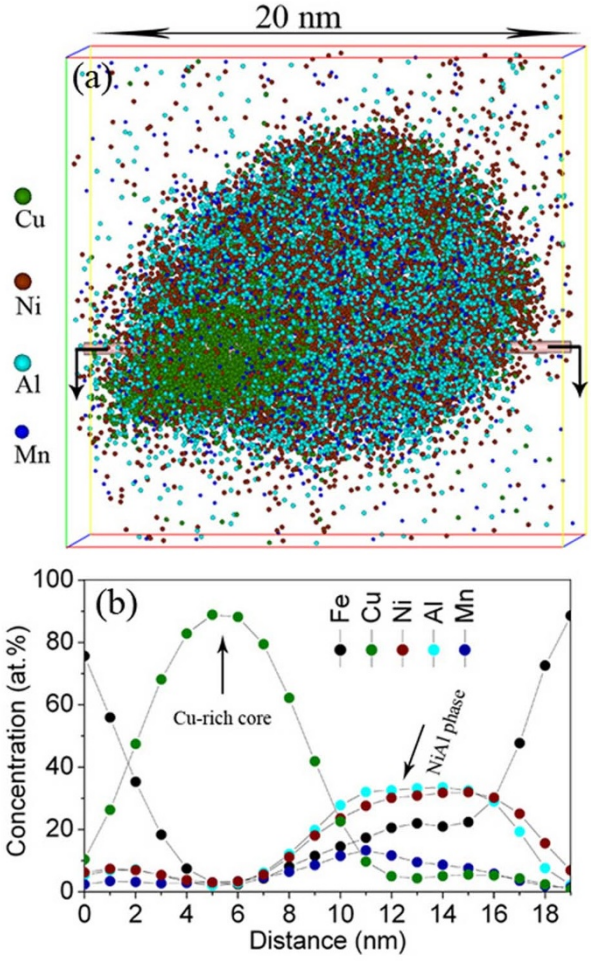


**Figure 4 | APT atom map (a) along with the one-dimensional concentration profiles (b) of a duplex precipitate in the high nickel alloy after aging at 500°C for 2000 h.** Both atom maps and concentration profiles show that Cu mainly enriched at the precipitate core, whereas Ni and Al along with Mn atoms were expelled away from the small Cu-rich core, resulting in the formation of the NiAl(Mn) phase.

Having established the elemental partitioning and structure of the precipitates, we thus attempted to elucidate the hardening mechanism in the high and low Ni alloys. It is well known that precipitate-hardening is governed by the interaction of moving dislocations and precipitates[28]. The increase in material strength associated with precipitate strengthening is given by the equation below[29]:

$$\Delta\sigma_{YS} = M\gamma R/bL, \tag{1}$$

where $\Delta\sigma_{YS}$ is the increment in yield strength associated with the precipitation strengthening, $\gamma$ is the apparent surface energy, $R$ is the precipitate radius, $b$ is the Burgers vector (~0.25 nm), and $M$ is the Taylor factor, which is ~3 for bcc materials[30]. $L$ is the mean precipitate spacing in the slip plane of the dislocation which can be calculated according to the equation[31]

$$L = 0.866 \times (RN)^{-1/2}, \tag{2}$$

where $R$ and $N$ are the average precipitate radius and number density. Given $R$ = 1.3 and 1.6 nm, as determined by APT for the low and high nickel alloys, respectively, and N = $3.6 \times 10^{24} m^{-3}$, the mean precipitate spacing,$L$ was found to be 12.7 and 11.4 nm for the low and high nickel alloys, respectively. Thus, substituting the increments in the yield strength (433 Mpa for the low nickel alloy and 628 MPa for the high nickel alloy) into Eq.1, the apparent surface energy ~0.35 J/m$^2$ and ~0.37 J/m$^2$ can be obtained for the low and high nickel alloys, respectively. The dislocation cutting-through model used here (Eq.1) gives the same apparent surface energy for both alloys within the experimental errors, suggesting that the structural features of the nanoscale precipitates in both alloys are similar. This is reasonable as B2-ordered NiAl domains have been observed even when Cu, Ni, Mn and Al elements cosegregate, forming B2-ordered domains and Cu-enriched domains[32]. However, nanoscale precipitates in the high Ni alloy have a co-precipitation structure with Cu-enriched core partially encased by B2-ordered Ni (Al, Mn) phase. This co-precipitation increases the precipitate size while maintaining the same number density, as compared to the low Ni alloy. Thus, in the context of the dislocation cut-through model, the increased yield strength in the high nickel alloy is mainly due to the precipitate size effect.

From APT and EELS mapping, the Ni-Al-enriched B2-ordered phase around the Cu-enriched core is a non-stoichiometric

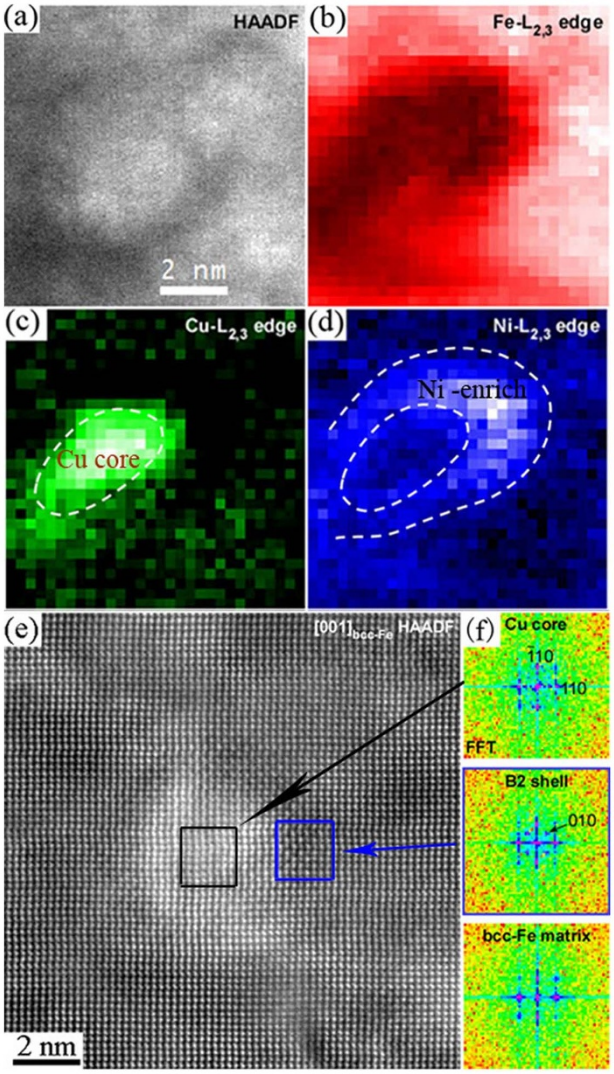


**Figure 5 | STEM-EELS elemental mappings of a duplex precipitate in the high nickel alloy after aging at 500°C for 10 h in vacuum.**
(a) HAADF-STEM image, (b) Fe-L2,3, (c) Cu-L2,3 and (d) Ni-L2,3, (e) Low-pass filtered high resolution [001]α-Fe HAADF image of a duplex precipitate with a Cu core partially encased by a B2-ordered phase in the high nickel alloy after aging at 500°C for 10 h in vacuum. The FFT pattern of bright Cu-rich core shows a distorted bcc structure, whereas the FFT pattern of the dark Ni(Mn, Al) phase (blue box) shows ordered 010B2 reflection indicating that the Ni(Mn, Al) phase has a B2 structure.

intermetallic compound with a broad composition range. This deviation from the stoichiometric composition due to the presence of substitutional elements can enhance local disordering and dislocation climbing or cutting, making the non-stoichiometric Ni-Al-enriched phase ductile[33]. The ductility of the NiAl phase can also be enhanced by superlattice dislocation movement which consists of two or more unit dislocations connected by an antiphase boundary[34]. The high lattice coherency of the co-precipitation structure with the bcc ferritic matrix and the superlattice dislocation can accommodate the extra energy needed to create antiphase boundaries, and making it easier for dislocation to cut through the nanoscale co-precipitates. Moreover, the formation of co-precipitation structure gives rise to a low interface energy between the precipitates and matrix. The low interface energy, along with the B2-Ni(Mn, Al) phase, is effective in stabilizing the precipitates. These results indicate that the development of a co-precipitation structure in this alloy allowed the particle size to grow while maintaining the same high number density, thereby increasing the strength without sacrificing the ductility. Importantly, this study has demonstrated that structure of nanoscale precipitates can be controlled through a small change in the alloy composition. Thus, this approach points a new direction in the design of alloys with both high strength and high ductility.

In summary, this study demonstrates a substantial improvement in yield strength without the sacrificing ductility by introducing nanoscale co-precipitates in Fe-based alloys. The atomic-scale observations by the combination of two complementary state-of-the-art microstructural characterization techniques of APT and Cs-corrected transmission electron microscopy provide compelling evidence that a co-precipitation structure with a Cu-enriched bcc core with a B2-ordered Ni(Mn,Al) phase formed around the core can be controlled through a small change in Ni content. The high lattice coherency of the co-precipitates with the bcc ferritic matrix contributes to the stability of high-density nanoparticles during aging treatments. This optimized combination of the precipitate size and the number density results in extremely high yield strength without sacrificing ductility. These findings offer insights into interactions between nano-scale precipitates and dislocations and have important implications in developing novel nano-scale PH alloys for structural applications.

## Methods

Fe-2.5Cu-2.1Al-1.5Mn (at.%)-based ferritic alloys with additional 2.5% Ni (denoted as the low nickel alloy) and 4% Ni (denoted as the high nickel alloy) were prepared by arc melting high-purity elemental metals (99.95 Fe, 99.8 Mn, 99.99 Ni, 99.99 Cu, 99.99 Al wt%). The detailed casting process was introduced elsewhere[13]. The specimens were solutionized at 900°C for 1 h in air and quenched in water after thermomechanical treatment. The specimens were aged subsequently at 500°C for 10 h in vacuum and a high nickel alloy was also aged at 500°C for 2000 h in air.

A neutron powder diffraction technique was used to determine the phases in the specimens using the VULCAN beamline at the Spallation Neutron Source, Oak Ridge National Laboratory[35]. The microstructure was observed by optical microscopy. Tensile specimens with gauge sizes of $12.5 \times 3 \times 0.75$ mm were tested on an Instron 5565 testing machine at room temperature in air at a strain rate of 0.004 $s^{-1}$. APT was performed with a Cameca Instruments (formerly IMAGO Scientific Instruments) local electrode atom-probe (LEAP 4000X HR) in voltage-pulsing mode. The Image Visualization and Analysis Software (IVAS) version 3.6 was used for 3-D reconstruction and composition analyses and to create isoconcentration surfaces. A 200-keV aberration-corrected JEOL JEM-2100F scanning transmission electron microscope (STEM) was applied with double spherical aberration correctors for both the probe-forming and image-forming lenses.. High angle annular dark field (HAADF) images, where the contrast is proportional to the square of atomic number, were acquired with an annular-type STEM detector. HAADF-STEM image simulations were performed for the constructed model using software of STEM for win HREM code (HREM Research Inc.).


1. Ardell, A. J. & Ozolins, V. Trans-interface diffusion-controlled coarsening. *Nat. Mater.* **4**, 309–316 (2005).
2. Clouet, E. *et al.* Complex precipitation pathways in multicomponent alloys. *Nat. Mater.* **5**, 482–488 (2006).
3. Hirata, A. *et al.* Atomic structure of nanoclusters in oxide-dispersion-strengthened steels. *Nat. Mater.* **10**, 922–926 (2011).
4. Mao, Z. G. *et al.* Themechanism of morphogenesis in a phase-separating concentrated multicomponent alloy. *Nat. Mater.* **6**, 210–216 (2007).
5. Radmilovic, V. *et al.* Highly monodisperse core-shell particles created by solid-state reactions. *Nat. Mater.* **10**, 710–715 (2011).
6. Kolli, R. P. & Seidman, D. N. The temporal evolution of the decomposition of a concentrated multicomponent Fe-Cu-based steel. *Acta Mater.* **56**, 2073–2088 (2008).
7. Dhua, S. K., Mukerjee, D. & Sarma, D. S. Influence of tempering on the microstructure and mechanical properties of HSLA-100 steel plates. *Metall. Mater. Trans. A* **32**, 2259–2270 (2001).
8. Lu, K., Lu, L. & Suresh, S. Strengthening Materials by Engineering Coherent Internal Boundaries at the Nanoscale. *Science* **324**, 349 (2009).
9. Fine, M. E. & Isheim, D. Origin of copper precipitation strengthening in steel revisite. *Scripta Mater.* **53**, 115–118 (2005).
10. Fine, M. E. *et al.* A New Paradigm for Designing High-Fracture-Energy Steels. *Metall. Mater. Trans. A* **41A**, 3318–3325 (2010).
11. Vaynman, S. *et al.* High-strength low-carbon ferritic steel containing Cu-Fe-Ni-Al-Mn precipitates. *Metall. Mater. Trans. A* **39A**, 363–373 (2008).
12. Zhang, Z. W. *et al.* Boron effects on the ductility of a nano-cluster-strengthened ferritic steel. *Mater. Sci. Eng. A* **528**, 855–859 (2011).

13. Zhang, Z. W. *et al*. Influence of Aging and Thermomechanical Treatments on the Mechanical Properties of a Nanocluster-Strengthened Ferritic Steel. *Metall. Mater. Trans. A* **43A**, 351–359 (2012).
14. Fujii, K. *et al*. Hardening and microstructural evolution in A533B steels under high-dose electron irradiation. *J. Nucl. Mater.* **340**, 247–258 (2005).
15. Goodman, S. R., Brenner, S. S. & Low, J. R. FIM-atom probe study of precipitation of copper from iron-1.4 at pct copper .1. field-ion microscopy. *Metall. Trans.* **4**, 2363–2369 (1973).
16. Isheim, D., Kolli, R. P., Fine, M. E. & Seidman, D. N. An atom-probe tomographic study of the temporal evolution of the nanostructure of Fe-Cu based high-strength low-carbon steels. *Scripta Mater.* **55**, 35–40 (2006).
17. Kolli, R. P., Mao, Z., Seidman, D. N. & Keane, D. T. Identification of a Ni(0.5)(Al(0.5-x)Mn(x)) B2 phase at the heterophase interfaces of Cu-rich precipitates in an alpha-Fe matrix. *Appl. Phys. Lett.* **91** (2007).
18. Miller, M. K. & Russell, K. F. Embrittlement of RPV steels: An atom probe tomography perspective. *J. Nucl. Mater.* **371**, 145–160 (2007).
19. Monzen, R., Iguchi, M. & Jenkins, M. L. Structural changes of 9R copper precipitates in an aged Fe-Cu alloy. *Phil. Mag. Lett.* **80**, 137–148 (2000).
20. Murayama, M., Katayama, Y. & Hono, K. Microstructural evolution in a 17-4 PH stainless steel after aging at 400 degrees C. *Metall. Mater. Trans. A* **30**, 345–353 (1999).
21. Othen, P. J., Jenkins, M. L. & Smith, G. D. W. High-resolution electron-microscopy studies of the structure of Cu precipitates in alpha-Fe. *Philos. Mag. A* **70**, 1–24 (1994).
22. Thompson, S. W. & Krauss, G. Copper precipitation during continuous cooling and isothermal aging of A710-type steels. *Metall. Mater. Trans. A* **27**, 1573–1588 (1996).
23. Zhang, Z. W. *et al*. From embryos to precipitates: A study of nucleation and growth in a multicomponent ferritic steel. *Phys. Rev. B* **84**, 174114 (2011).
24. Pareige, P. J., Russell, K. F. & Miller, M. K. APFIM studies of the phase transformations in thermally aged ferritic FeCuNi alloys: Comparison with aging under neutron irradiation. *Appl. Surf. Sci.* **94-5**, 362–369 (1996).
25. Zhang, C. & Enomoto, M. Study of the influence of alloying elements on Cu precipitation in steel by non-classical nucleation theory. *Acta Mater.* **54**, 4183–4191 (2006).
26. Schnitzer, R., Schober, M., Zinner, S. & Leitner, H. Effect of Cu on the evolution of precipitation in an Fe-Cr-Ni-Al-Ti maraging steel. *Acta Mater.* **58**, 3733–3741 (2010).
27. Anderson, I. M., Duncan, A. J. & Bentley, J. Site-distributions of Fe alloying additions to B2-ordered NiAl. *Intermetallics* **7**, 1017–1024 (1999).
28. Smallman, R. E. & Ngan, A. H. W. *Physical Metallurgy and Advanced Materials (Seventh edition)*. (Elsevier Ltd., Imprint in Burlington, 2007).
29. Haasen, P. *Mechanical properties of solid solutions.* (Elsevier Science BV, Amsterdan-Lausanne-New York-Oxford-Shannon-Tokyo, 1996).
30. Doner, M., Chang, H. & Conrad, H. Stress-strain behavior and dislocation-structure at small strains in iron deformed in tension, torsion and combined tension-torsion. *Metall.Tran.* **6A**, 1017–1028 (1975).
31. Russell , K. C. & Brown, L. M. *Acta Metall. Mater.* **20**, 969 (1972).
32. Wen, Y. R. *et al*. Microstructure characterization of Cu-rich nanoprecipitates in a Fe-2.5 Cu-1.5 Mn-4.0 Ni-1.0 Al multicomponent ferritic alloy, Acta Materialia, 10.1016/j.actamat.2012.12.034.
33. Ball, A. & Smallman, R. E. The deformation properties and electron microscopy studies of the intermetallic compound NiAl. *Acta Metallurgica* **14**, 1349–1355 (1966).
34. Stoloff, N. S. & Davies, R. G. The Mechanical Properties of Ordered alloys. *Prog. Mater. Sci.* **13**, 1–86 (1968).
35. Wang, X. L. *et al*. VULCAN - The engineering diffractometer at the SNS. *Physica. B* **385**, 673–675 (2006).

## Acknowledgements

This research was supported by internal funding from Auburn University (ZWZ, BAC) and City University of Hong Kong (CTL and XLW). Atom Probe Tomography (MKM) at the Oak Ridge National Laboratory ShaRE User Facility was sponsored by the Scientific User Facilities Division, Office of Basic Energy Sciences, U.S. Department of Energy. Neutron diffraction benefitted from the use of the Spallation Neutron Source, which is sponsored by the Division of Scientific User Facilities, Office of Basic Energy Sciences, U.S. Department of Energy. ZWZ was supported in part by the NSFC Funding (No. 51171081) and RFDP Funding (No. 20113219120044) for the sample preparation. ZWZ also acknowledges Dr. D. Ma of Oak Ridge National Laboratory for the useful discussions. MWC, TF and AH acknowledge the support of JST, PRESTO, 4-1-8 Honcho Kawaguchi, Saitama 332-0012, Japan.

## Author contributions

Z.W.Z. designed and conducted the experiments, collected and analyzed the mechanical and APT data, discussed the results and drafted the manuscript. C.T.L. supervised the overall project, designed the experiments, discussed the results and helped in drafting the manuscript. M.K.M. collected and analyzed APT data, discussed the results and wrote a part of the manuscript. X.L.W. designed the diffraction experiments, discussed the results and helped in drafting the manuscript. Y.R.W., T. F., A. H. and M.W. C. collected and analyzed the STEM data. G.C. and B.A.C. helped with the experiments and discussed the results. All the authors read and commented on the manuscript.

## Additional information

**Competing financial interests:** The authors declare no competing financial interests.



**How to cite this article:** Zhang, Z.W. *et al*. A nanoscale co-precipitation approach for property enhancement of Fe-base alloys. *Sci. Rep.* **3**, 1327; DOI:10.1038/srep01327 (2013).